Surface ordering at the air-nematic interface. Part 2: a spectroscopic ellipsometry study of orientational order[♦]

Y.G.J. Lau[1], Susanne Klein, Christopher J.P. Newton, Robert M. Richardson[2]
Media Technologies Laboratory
HP Laboratories Bristol
HPL-2006-168
November 30, 2006*

order parameter, air-nematic interface, ellipsometry

Spectroscopic ellipsometry has been used to measure enhanced orientational ordering at the nematic-air interface of 8CB as the smectic-A phase was approached by cooling from the isotropic phase. The depth profile of the orientational order has been estimated by calculating the ellipsometric parameters for a homeotropic uniaxial surface film on a uniaxial subphase using the Abelès matrix method. This showed that the depth of the enhanced orientationally ordered region was ~ 10nm at 0.5°C above the nematic-smectic-A transition. This is substantially less than the thickness of the region with surface enhanced smectic order as determined by neutron reflection and a model of the surface structure consistent with both sets of results is proposed.

Surface ordering at the air-nematic interface. Part 2: a spectroscopic ellipsometry study of orientational order

Lau Y. G. J. [a, b], Klein S. [c], Newton C. J. P. [c], Richardson R. M.[b]

[a] Institut Laue-Langevin

6 Rue Jules Horowitz, BP 156 – 38042 Grenoble, Cedex 9, France.

[b] H. H. Wills Physics Laboratory

Royal Fort, Tyndall Avenue, Bristol, BS8 1TL, U.K.

[c] Hewlett-Packard Laboratories

Bristol, BS34 8QZ, UK.

Abstract

Spectroscopic ellipsometry has been used to measure enhanced orientational ordering at the nematic-air interface of 8CB as the smectic-A phase was approached by cooling from the isotropic phase. The depth profile of the orientational order has been estimated by calculating the ellipsometric parameters for a homeotropic unaxial surface film on a uniaxial subphase using the Abelès matrix method. This showed that the depth of the enhanced orientationally ordered region was ~ 10nm at 0.5°C above the nematic-smectic-A transition. This is substantially less than the thickness of the region with surface enhanced smectic order as determined by neutron

reflection and a model of the surface structure consistent with both sets of results is proposed.

1. Introduction

The knowledge of liquid crystal molecular structure at an interface has direct applications in liquid crystal devices, as well as increasing understanding in adsorption and wetting phenomena. In the last two decades, surface-induced organisation of liquid crystals at interfaces has been an active area research using various techniques including ellipsometry [1], atomic force microscopy [2], X-ray and neutron reflectometry [3,4].

Ellipsometric measurements at the air/liquid crystal interface have shown that there is pre-transitional ordering at the surface above the isotropic-nematic bulk transition [1]. It has been shown that smectic layering is induced in nematic liquid crystals close to the nematic-smectic-A phase transition at the air/liquid crystal interface [3] and at solid substrates [4]. An ellipsometer uses a polarized light beam that is reflected from the surface of interest. The measured change in polarization, both in amplitude and phase, can be used to deduce the properties of the interface. This process requires modelling of the data in order to gain useful information such as refractive indices and film thicknesses. This often involves trial and error and one needs a model that accurately describes the surface to get good fits to data and determine parameters of interest.

Ellipsometry offers complimentary information to neutron reflection. Cold neutrons have a sub-nanometre wavelength and so a scattering vector (Q) of up to ~ 3 nm^{-1} is currently typical using reflection geometry. This is adequate to probe any

translational order at the nematic-air surface due to smectic layers which typically have a repeat distance of 3 nm and give a pseudo-Bragg peak at $Q \sim 2.0 \text{ nm}^{-1}$. Reflection of visible light has the disadvantage that it cannot observe features such as smectic layers since the Q-range reached is limited by the wavelength of the incident beam, so that the maximum Q is of order of 10^{-2} nm^{-1}. However, ellipsometry has greater precision than simple reflectivity since it measures accurately the change of polarization rather than just the reflected intensity. So although it cannot spatially resolve structures less than a few hundred nanometres, ellipsometry is remarkably sensitive to changes in birefringence and thickness of films near the surface of the sample, and is therefore sensitive to surface enhanced orientational order.

The electric field of linearly polarized light can be decomposed into vector components perpendicular and parallel to the plane of incidence. These are known as the s and p components respectively. Details of polarized light can be found elsewhere [5]. The resulting change in polarization upon reflection at an interface is expressed as the ellipsometric parameter, ρ, which is a complex number defined by

$$\rho = \frac{R_p}{R_s} \qquad (1)$$

where R_p and R_s are the Fresnel coefficients for reflection of the p- and s-components. The ellipsometric parameter is measured and is often displayed as the ellipsometric angles Ψ and Δ where $\Psi = \tan^{-1}|\rho|$ represents the amplitude change and $\Delta = \tan^{-1}|\Im m(\rho)/\Re e(\rho)|$ represents the phase change on reflection.

It is important to realize that the *p*- and *s*- components reflect differently from the interface depending on the angle of incidence. At zero incident angles (to the interface normal) the light source is directly above the sample and there is low reflectance. When the angle approaches 90° the light shines nearly parallel to the sample and the reflectance is high. Ellipsometry is concerned with the whole range of angles between 0 and 90°. As the angle of incidence increases, R_s steadily increases from a small value but R_p starts out at a small value and then decreases until it reaches zero at the Brewster angle, θ_B, before increasing again. In the case of an idealized sharp interface between two homogeneous dielectrics, the phase difference Δ jumps by 180° and the amplitude ratio $\tan \Psi = \rho = |r_p|/|r_s|$ is equal to zero because the *p*-polarized light is not reflected at θ_B. For a real interface, Δ is continuous and $\tan \Psi$ does not drop to zero. Surface roughness or additional surface layers shift $\tan \Psi$ from zero. The main importance of the Brewster angle is that R_p is zero for an ideal interface and any additional structure at the interface causes R_p to become finite. Hence, Brewster angle ellipsometry is very sensitive to any additional films at the surface. For material properties that are temperature dependent, it is also informative to probe the shift of the Brewster angle with temperature since its value depends on the bulk refractive indices.

Beaglehole was one of the first to measure ρ for the air – 4-pentyl-4'- cyanobiphenyl (5CB) interface as a function of temperature [1]. The value of the Brewster angle also changed on approaching T_{NI} due to the change in bulk birefringence. Beaglehole related R_p / R_s to the surface order by considering the dielectric constants well outside and inside the liquid close to θ_B. Kasten *et al* later went further by extending measurements to a homologous series of *n*CB liquid crystals at the free surface [6]. The results in the isotropic phase show that complete

wetting by a homeotropically aligned nematic film occurs for $n = 6, 7, 8$ while for $n = 5$ the wetting layer remains finite at T_{NI}. In the nematic phase, they found enhanced orientational order at the 7CB and 8CB surfaces. A value of $S_{surface} / S_{bulk} = 1.35 \pm 0.07$ was reported where $S_{surface}$ is the value at the surface and S_{bulk} is the value in the bulk phase. Other researchers have also made investigations on these systems in the isotropic phase [7,8,9].

In these previous researches, a single wavelength incident light was used. In the work reported here, a spectroscopic ellipsometer has been used. Spectroscopic ellispsometry offers many advantages over the single-wavelength method, i.e. it has multilayer capabilities, depth profile of optical properties, and solutions of otherwise unsolvable material problems. Here, measurements at the free surface of 4-octyl-4-cyanobiphenyl (8CB) are reported using a commercial spectroscopic ellipsometer. Scans over wavelength as well as angle can, in principle, provide more independent data points so that it is possible to distinguish between similar models. The results also compliment neutron reflectometry data given in a previous publication[10].

2. Theoretical background

The birefringence, Δn, of a nematic liquid crystal may, to a good approximation, be assumed to be proportional to the orientational order parameter, S, which is a function of temperature [11]

$$\Delta n(T) = n_e(T) - n_o(T) = (\Delta n)_0 S(T) \tag{2}$$

where n_e and n_o are the refractive indices for propagation parallel and perpendicular to the liquid crystal director and $(\Delta n)_0$ is the birefringence in a perfectly ordered state (e.g. at $T = 0K$). Note that the order parameter S is more correctly proportional to the difference in the squares of the two refractive indices $n_e^2 - n_o^2$ but for small values of $n_e - n_o$ equation (2) is valid. The average refractive index is defined as

$$\bar{n} = \frac{1}{3}(n_e + 2n_o)$$

(3)

By combining equations the birefringence $\Delta n = n_e - n_o$ and equation (3), the ordinary and extraordinary refractive indices can be written as

$$n_o = \bar{n} - \frac{1}{3}\Delta n$$

(4)

$$n_e = \bar{n} + \frac{2}{3}\Delta n$$

(5)

It is useful to relate the birefringence at the surface of a nematic to the orientational order parameter at the surface. This may be done by defining the ratio of the surface to bulk order parameters, S_R,

$$S_R = \frac{S_{surface}}{S_{bulk}} = \frac{\Delta n_{surface}}{\Delta n_{bulk}} = \frac{\Delta n_{bulk} + \gamma}{\Delta n_{bulk}}$$

(6)

where γ is the excess birefringence at the surface. Thus, if the bulk birefringence and the bulk order parameter are known, the surface excess birefringence, γ, (determined by ellipsometry) may then be used to calculate the surface orientational order parameter.

In this work the ellipsometric parameter from a surface region with enhanced birefringence on top of an anisotropic bulk phase is analysed. (See figure 1.) Studies of anisotropic films on anisotropic substrates have not been common so the theory to model the ellipsometric parameters is not extensively reported. The well-known Berreman method applies to a uniaxial material with any director distribution [12] but it only describes systems where both ambient phases, i.e. the incident and bulk media, are isotropic. Thus some care in the choice of a suitable theory for the data analysis in this paper has been necessary.
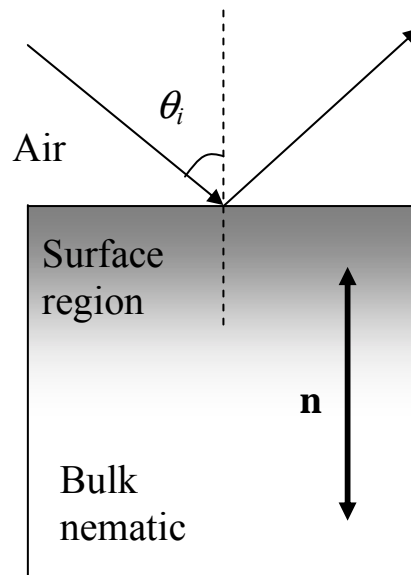

Figure 1 Schematic view of the air-liquid crystal interface to show the incident medium (air), the surface region and the bulk phase or subphase. The double arrow represents the director. The angle of incidence is θ_i.

In early studies, the optical behaviour of films with uniaxial anisotropy on top of isotropic substrates was explored [13]. More recently, Odarich [14,15] has given a theoretical approach to calculating ellipsometric parameters for anisotropic films on anisotropic substrates and he has pointed out the flaws in some of the previous attempts [5,16]. He considered reflection of light from the interface between two anisotropic media and discussed the Fresnel coefficients for two separate cases: the optical axis perpendicular to the plane of incidence and optical axis perpendicular to the boundary surface. Recently, one of us (C.N.) has derived results for a uniaxial film on top of a uniaxial bulk phase which apply whenever the director remains in the plane of incidence. These reduce to those given by Odarich and thus include the nematic system with homeotropic boundary conditions studied in this work.

The ellipsometric data has been compared with values calculated for simple models of the excess birefringence at the nematic-air surface. The refractive indices have been assumed to be wavelength dependent following the Cauchy formula[17]

$$n_{o,e} = a_{o,e} + \frac{b_{o,e}}{\lambda^2} \ .$$

(7)

Parameters a and b have been determined from wavelength dependent measurements of the bulk refractive indices using an Abbé refractometer. The results for parameters a and b for bulk 8CB are shown in table 1.

T - T_{NA} / °C	a_{o3}	b_{o3} / nm^2	a_{e3}	b_{e3} / nm^2
10.5	1.529	12500		
9.5	1.529	12500		
8.5	1.529	12500		
7.5	1.530	12500		
6.5	1.500	10000	1.596	19000
5.5	1.500	9000	1.602	19000
4.5	1.494	10200	1.610	18000
3.5	1.497	9000	1.609	19500
2.5	1.495	9000	1.613	19500
1.5	1.494	9000	1.613	20600
0.5	1.493	9000	1.619	20600

Table 1 Cauchy parameters for 8CB found from fits to Abbé refractomer measurements using wavelengths 451.5, 539, 547, 579, 632 and 648nm. Temperatures more than 7°C above the transition are in the isotropic phase.

Two different functions are used to describe the refractive indices of the surface film: the exponentially decaying profile and the truncated layer profile. For the exponentially decaying profile, the refractive indices are given by

$$n_o(z) = n_{o,bulk} - \frac{1}{3}\gamma\exp\left(\frac{-z}{\xi_s}\right) \tag{8}$$

$$n_e(z) = n_{e,bulk} + \frac{2}{3}\gamma\exp\left(\frac{-z}{\xi_s}\right) \tag{9}$$

and for the truncated layer model by

$$n_o(z) = n_{o,bulk} - \frac{1}{3}\gamma\left(\frac{1}{2} - \frac{1}{2}erf\left[\frac{z - \xi_s}{\sigma}\right]\right) \tag{10}$$

$$n_e(z) = n_{e,bulk} + \frac{2}{3}\gamma\left(\frac{1}{2} - \frac{1}{2}erf\left[\frac{z-\xi_s}{\sigma}\right]\right) \tag{11}$$

where $erf(z)$ is the standard error function, ξ_s is the thickness of the film, and σ is the width of the truncation. When $\sigma << \xi_s$ equations 10 and 11 describe a uniform layer and when $\sigma \sim \xi_s$ they describe a more gradual decay of the excess birefringence. The relative wavelength dependence of the refractive indices was kept the same as for the bulk.
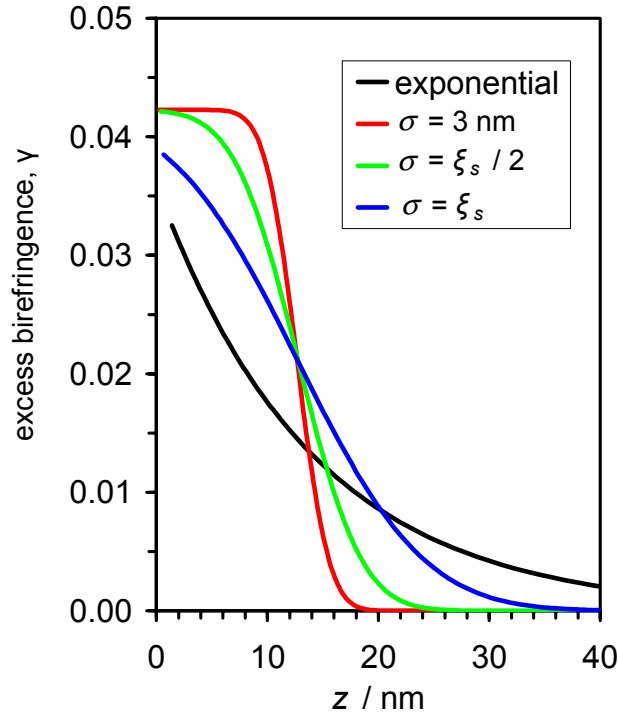

Figure 2 The depth profiles used to model the excess birefringence: the exponential decay and three truncated profiles. The truncation takes place abruptly over one smectic layer spacing, 3 nm, giving a uniform film or more gradually over half or the full film thickness, ξ_s giving decaying films.

Figure 2 shows the excess birefringence due to the different models used to fit the ellipsometric data. These are the exponential decaying profile, the uniform layer where the truncation takes place abruptly over one smectic layer spacing (i.e.

$\sigma = 3$ nm) and two profiles with a more gradual truncation taking place over half the thickness of the film (i.e. $\sigma = \xi_s/2$) and the full thickness of the film (i.e. $\sigma = \xi_s$). The ellipsometric parameters were calculated by dividing the surface into strata using the Abelès matrix method [18]. This is described in full in the appendix.

3. Experimental procedure

A thin liquid crystal film of 8CB of approximately 1mm thick was placed on top of a rough silicon wafer. The rough silicon ensured that no back reflections would reach the detector. The wafer was then placed on top of a heating stage which allowed the measurements in the isotropic through to the nematic and smectic phases to be made. The ellipsometer used was an M-2000U™ Spectroscopic Ellipsometer (J. A. Woollam Co. Inc.) [19,20]. This is a rotating compensator ellipsometer. Scans of incident angle were made in the wavelength spectrum between $500 - 1000$nm.

4. Results

Figure 3 shows the results for Ψ and Δ data respectively as a function of temperature and incident angle at a selected wavelength of 700nm. A shift in the Brewster angle θ_B is seen with change of temperature, with a discontinuous jump from 57.3º to 55.5º corresponding to the I-N bulk phase transition. The transition temperature T_{NI} was found to be $T_{NI} = (41.5 \pm 0.5)$ºC. On cooling the isotropic phase towards the transition, there is a marked increase in the minimum value of Ψ and the step in Δ becomes less sharp. This suggests that a birefringent surface layer is growing in the isotropic phase. At temperatures below the transition the minimum

value of Ψ is lower and the step in Δ becomes sharper again. This is believed to be the result of smaller difference in the optical properties of the surface and the nematic bulk. To quantify the excess birefringence and thickness of the surface region, the Ψ and Δ data were fitted by the models discussed above.

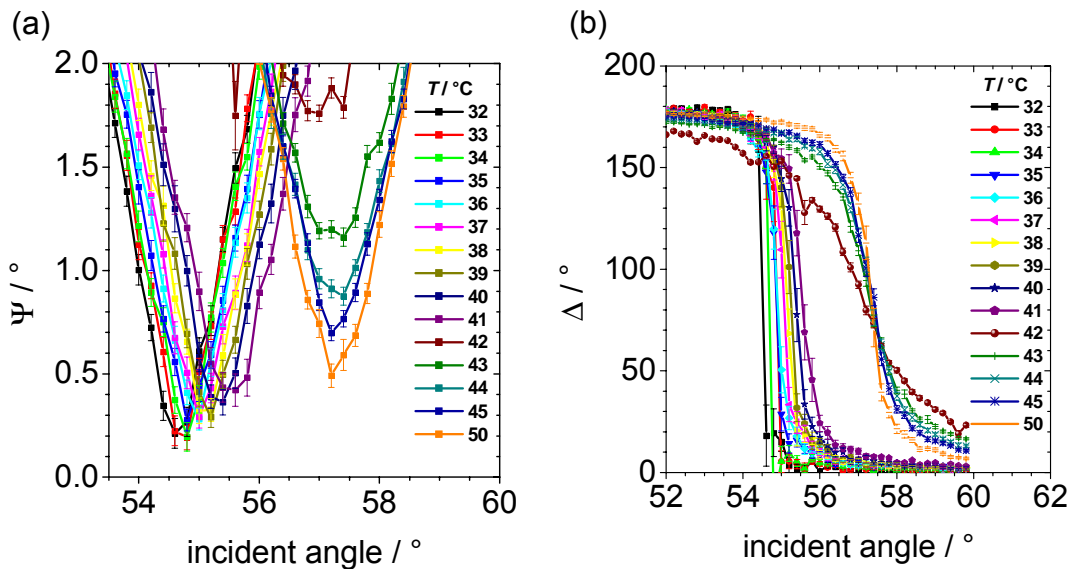**Figure 3** (a) Ψ and (a) Δ as function of incident angle at some temperatures (cooling down) at 700nm. The discontinuous shift in Brewster angle defines the I-N bulk phase transition and lies between 41 and 42°C. (The lines are to guide the eye only).

The models were calculated using the Abelès matrix formulism [18] described the appendix and the fitting was using the VA05A Harwell subroutine [21] to minimise χ^2. The raw data for both Ψ and Δ consisted of 12600 data points at closely spaced wavelengths. These data were regrouped by combining seven adjacent values into one data point so that a data set of 1800 points was used for further analysis. In fitting the ellipsometric data from the nematic, it was usually impossible to find a unique minimum χ^2 by allowing both the surface film thickness and its excess birefringence to refine. To investigate this problem and to determine the acceptable ranges for these parameters, the value of the excess birefringence, γ, was systematically varied whilst allowing the film thickness, ξ_s, to refine. The bulk

refractive indices used were taken from the separate Abbé refractometer measurements (shown in table 1) and a small correction γ_b was introduced and allowed to refine to accommodate any temperature discrepancy between the Abbé refractometer and the ellipsometer.

$$n_{o,bulk} = n_{o,measured} - \frac{1}{3}\gamma_b \qquad\qquad (12)$$

$$n_{e,bulk} = n_{e,measured} + \frac{2}{3}\gamma_b \qquad\qquad (13)$$

The value of γ_b was always less than $\sim 3 \times 10^{-3}$ which corresponds to a temperature difference of less than 0.3°C. Figure 4 shows typical results from this procedure using the four models shown in figure 2 fitted to Ψ data or Δ data from a sample 1.5° above the nematic to smectic A transition. The figure shows reduced χ^2 and surface film thickness from the fit as a function of the assumed value of the excess birefringence γ.

From figure 4, there is clearly no minimum in the reduced χ^2 and a range of γ values give equally acceptable values of the reduced χ^2. For comparing the quality of fits with different values of γ , it was decided to use a 1% χ^2 probability criterion. For 1800 data points, the reduced χ^2 should be less than 1.08. However the reduced χ^2 from the fits were never that low with the models used. In order to make a consistent comparison of the acceptable ranges of the thickness parameter, it was decided to accept the range giving reduced χ^2 up to 8% above the lowest value found for each data set.
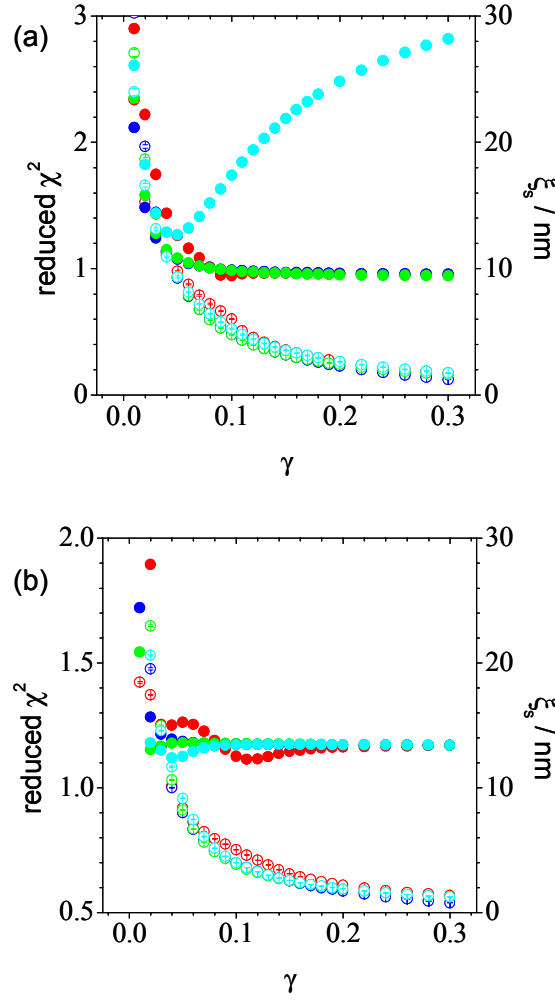
Figure 4 Results from fits to (a) Ψ and (b) Δ data at $T - T_{NA} = 1.5$ °C for all four film models: exponential (red), uniform (dark blue), $\sigma = \xi_s/2$ (green), $\sigma = \xi_s$ (light blue) (Reduced χ^2 = filled circles, film thickness = open circles).

Table 2 shows the values of acceptable surface thicknesses as found from the criterion of reduced χ^2 being within 8% of the lowest value. The ranges were determined from both Ψ and Δ data using four different surface film models.

Figure 4 suggests that only a thin and highly ordered film fits the results since a surface film with larger thickness and lower excess birefringence has significantly higher reduced χ^2. Figure 5 shows and example fit to Ψ and Δ as a function of wavelength using the exponential decay model for a temperature 1.5° above the nematic-smectic-A transition. It was found more convenient to inspect the fits as

superimposed wavelength scans for each angle of incidence rather than vice versa. It can be seen that the fitted lines are through or close to the error bars as expected for reduced χ^2 of ~1.5. We believe that the value of χ^2 obtained is not lower for instrumental reasons as a similar measurement on a non-mesogenic liquid produced a similar value of χ^2. Hence we are confident that the values for the thickness and excess birefringence in table 2 are significant.
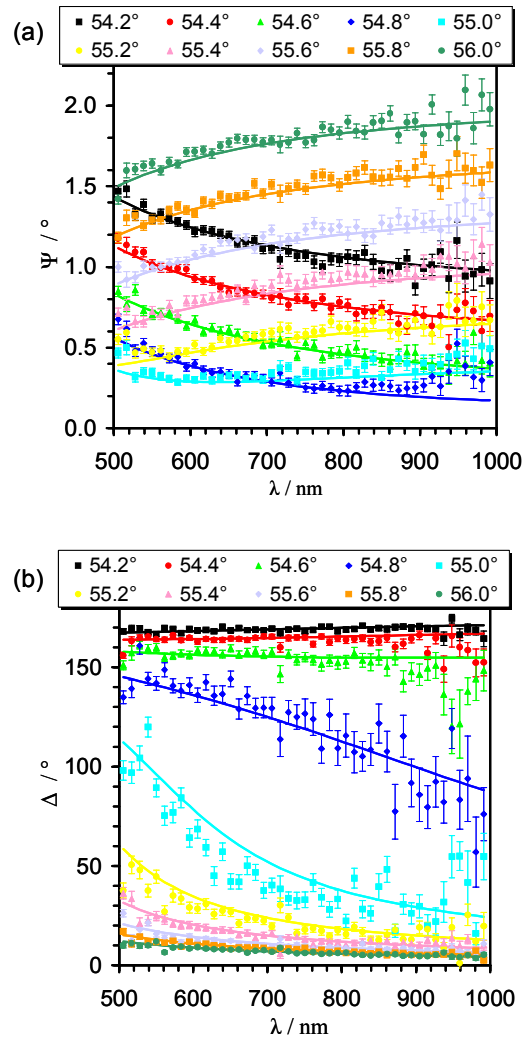

Figure 5 Fits of the exponential decay model to the Ψ and Δ data as a function of wavelength and angle of incidence. The sample temperature was 1.5° C above the transition to smectic A. For Ψ the general level of the lines goes through a minimum at the θ_B (~55.0°) and the slopes result from the wavelength dependence of the refractive indices which shifts θ_B. For Δ, the low angles are below the step down that occurs around θ_B and the high angles are above it. The data around θ_B (~55.0°) is most sensitive to the surface optical properties.

$T-T_{NA}$ / °C	exponential			σ = 3nm			σ = ξ_s/2			σ = ξ_s		
	ξ_s / nm	γ	S_R	ξ_s / nm	γ	S_R	ξ_s / nm	γ	S_R	ξ_s / nm	γ	S_R
	Ψ data											
10.5	5 - 7	0.15 - 0.24		9 - 15	0.07 - 0.12		8 - 13	0.08 - 0.13		6 - 11	0.1 - 0.16	
9.5	5 - 8	0.17 - 0.26		11 - 16	0.08 - 0.12		9 - 14	0.09 - 0.13		7 - 12	0.11 - 0.17	
8.5	6 - 9	0.2 - 0.28		13 - 16	0.1 - 0.13		12 - 15	0.11 - 0.14		9 - 12	0.13 - 0.19	
7.5	< 17	> 0.18		17 - 35	0.08 - 0.15		15 - 28	0.1 - 0.17		12 - 23	0.12 - 0.22	
6.5	< 3	> 0.27	> 2.2	< 9	> 0.17	> 1.4	< 8	> 0.18	> 1.5	< 5	> 0.2	> 1.7
5.5	< 3	> 0.31	> 2.4	< 3	> 0.27	> 2.1	< 4	> 0.25	> 1.9	< 3	> 0.29	> 2.2
4.5	5	0.16 - 0.2	1.2 - 1.4									
3.5	8	> 0.21	> 1.5	< 6	> 0.22	> 1.6	< 5	> 0.23	> 1.3	4 - 9	0.19 - 0.25	1.4 - 1.8
2.5	< 10	> 0.2	> 1.3	< 11	> 0.19	> 1.3	< 11	> 0.19	> 1.3	< 9	> 0.2	> 1.3
1.5	< 8	> 0.23	> 1.5	< 7	> 0.22	> 1.5	3 - 7	> 0.23	> 1.5	< 7	0.19 - 0.21	1.3 - 1.4
0.5	<10	> 0.27	> 1.7	< 7	> 0.22	> 1.4	3 - 7	0.22 - 0.34	1.4 - 2.1	< 7	> 0.21	> 1.3
	Δ data											
10.5	< 5	> 0.2		< 11	> 0.09		< 10	> 0.1		< 8	> 0.13	
9.5	< 6	> 0.22		< 12	> 0.1		< 11	> 0.11		< 9	> 0.14	
8.5	< 7	> 0.24		< 16	> 0.1		<14	> 0.11		< 11	> 0.14	
7.5	< 13	> 0.22		14 - 27	> 0.1		13 - 25	0.11 - 0.2		10 - 19	0.14 - 0.26	
6.5	< 3	> 0.28	> 2.3	< 9	> 0.17	> 1.4	< 6	> 0.19	> 1.6	< 4	> 0.22	> 1.8
5.5	< 4	> 0.24	> 1.9	<7	> 0.19	> 1.5	< 7	> 0.19	> 1.5	< 6	> 0.2	> 1.5
4.5	< 4	> 0.22	> 1.6	< 15	0.18 - 0.2	1.2 - 1.4	< 10	> 0.18	> 1.2	< 7	> 0.18	> 1.3
3.5	4 - 9	0.19 - 0.27	1.4 - 1.9	< 13	> 0.17	> 1.2	< 14	> 0.17	> 1.2	< 16	> 0.17	> 1.2
2.5	< 14	> 0.18	> 1.2	< 13	> 0.18	> 1.2	< 24	> 0.17	> 1.1	< 15	> 0.18	> 1.2
1.5	< 6	> 0.23	> 1.5	< 13	> 0.18	> 1.2	< 23	> 0.17	> 1.1	< 21	> 0.17	> 1.1
0.5	< 4	> 0.21	> 1.3	< 16	> 0.18	> 1.1	< 12	> 0.19	> 1.2	< 12	> 0.19	> 1.2

Table 2 Values of acceptble film thickness, ξ_s, and surface to bulk order parameter ratio, S_R, found by systematically varying the surface excess birefringence for the exponential decay model, the uniform film model, for a film with thickness truncation σ equal to half the film thickness, and for a film with σ equal to the full film thickness.

Table 3 shows the thicknesses of regions with surface smectic layering that have been determined using neutron reflectivity for all four surface film models. All four models give similar results. The thicknesses are much greater than found by ellipsometry. For instance, near the T_{NA} transition, the neutron reflection gives ~ 40 nm as compared to <10 nm from ellipsometry. The comparison between the values of the surface film thickness found by ellipsometry and those found by neutron reflection suggests that the surface enhanced nematic order does not extend into the bulk as far as the surface smectic layering. This suggests that although smectic layers exist near the surface, the orientational order of the molecules in the layers closest to the bulk is very similar to the bulk value. A schematic of this arrangement is shown in figure 6.

T-T_{NA} / °C	exponential ξ_s / nm	$\sigma = 3$ nm ξ_s / nm	$\sigma = \xi_s / 2$ ξ_s / nm	$\sigma = \xi_s$ ξ_s / nm
4.25	7 ± 2	12 ± 3	10 ± 3	7 ± 2
3.25	10 ± 4	19 ± 4	15 ± 3	11 ± 4
2.25	12 ± 2	16 ± 1	15 ± 2	12 ± 2
1.75	16 ± 5	25 ± 4	22 ± 6	17 ± 4
1.25	21 ± 4	34 ± 2	30 ± 4	23 ± 3
0.75	25 ± 5	38 ± 2	35 ± 4	26 ± 3
0.25	42 ± 10	56 ± 2	45 ± 3	35 ± 3

Table 3 Thickness (in nm) of surface smectic layering determined by neutron reflectivity for all surface film models.

The ranges of excess birefringence values giving acceptable values of χ^2 can be converted into surface relative order parameters, S_R, using equation (6) and these are also shown in table 2. The values suggest that the surface region has a highly enhanced orientational order parameter compared to the bulk value. For example, a typical S_R value of 1.6 and a value [22] of the bulk orientational order parameter of ~ 0.6, suggests that the surface region has an order parameter of ~ 1.0 (ie 1.6×0.6). Thus the ellipsometric results suggest a relatively thin (<10nm for exponential

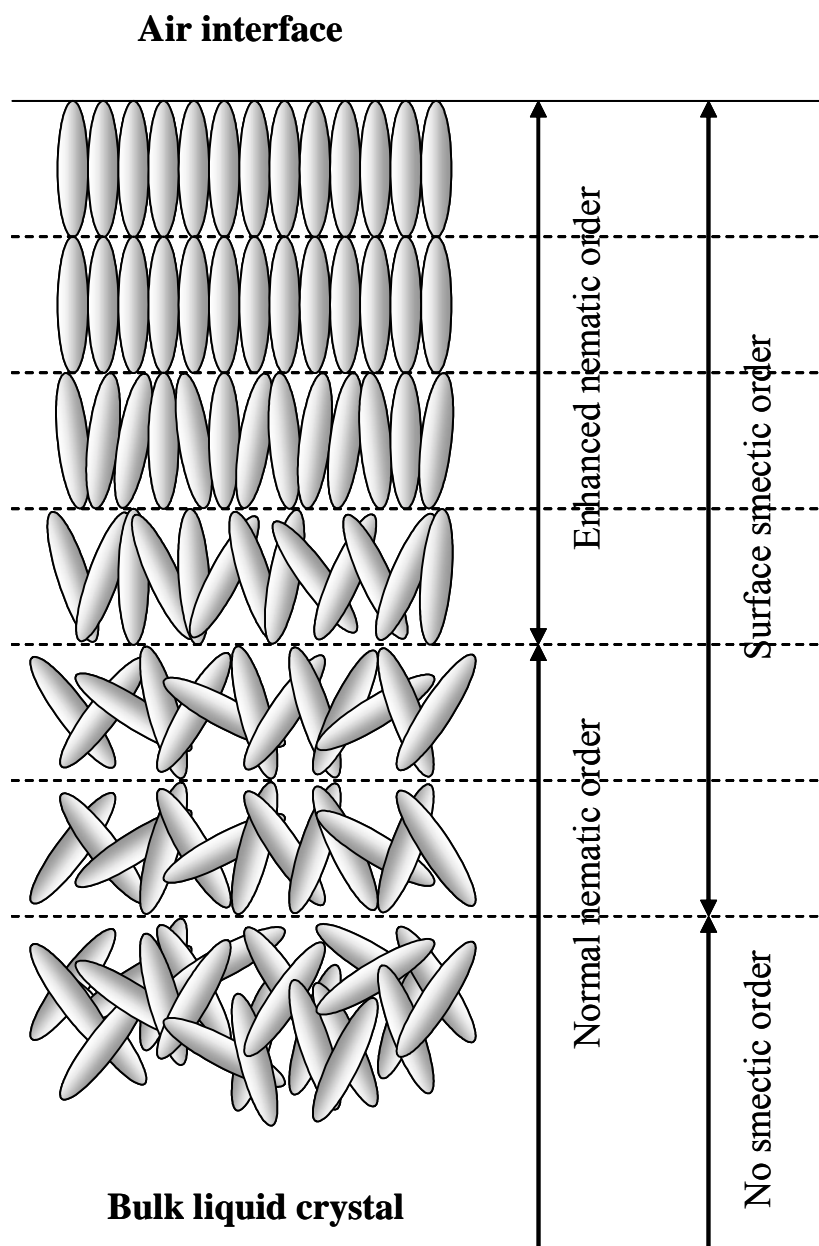model) but highly orientationally ordered surface region. This feature is also captured in the sketch in figure 6.

Air interface

Bulk liquid crystal

Figure 6 Schematic showing model of surface enhanced nematic order and surface smectic layering as deduced from ellipsometric and neutron reflectivity results. The smectic layering extends further into the bulk nematic than the enhanced orientational order.

A naïve picture would be that there is a region at the surface with enhanced nematic and smectic order. However the present results imply that the extent of surface orientational order is less than the extent of surface smectic layering at the

air-liquid crystal interface. This is a rather unexpected result since orientational and translational order are generally understood to be coupled (e.g. according to the McMillan theory [23]) and so increased smectic ordering would be accompanied by increased nematic order. However there is no contradiction. The neutron and ellipsometry results are both consistent with a thin region (<10nm) that has a high orientational order overlying a thicker region having translational order and rather weak enhancement of the orientational order due to the coupling.

5. Conclusion

Spectroscopic ellipsometry was used to investigate surface enhanced orientational order at the air-liquid crystal interface just above the onset of bulk smectic order. A comparison with a parallel set of neutron reflection measurements has shown that the surface smectic features penetrate further into the bulk nematic phase than most of the enhanced orientational order. A model that is consistent with both sets of experimental results is suggested. It is a strongly orientationally ordered region whose thickness is only a few smectic layers on top of a thicker region with smectic order exponentially decaying over tens of nanometres with only a small enhancement of the orientational order.

Appendix

The reflected amplitude for a single film is given by the standard formula

$$R_m = \frac{r_{\phi 1m} + r_{12m}\exp(i\beta_m)}{1 + r_{\phi 1m} r_{12m}\exp(i\beta_m)} \tag{A.1}$$

where subscripts m stand for either s- or p- polarizations, and '$\phi 1$' refer to the interface between media ϕ and 1, and '12' the interface between media 1 and 2. In order to proceed in calculating reflectivity for a uniaxial film on top of a uniaxial substrate, the following definitions are made

$$\zeta = n_\phi \sin\theta_i$$

$$\eta_\phi = \sqrt{n_\phi^2 - \zeta^2}$$

$$\eta_{o1} = \sqrt{n_{o1}^2 - \zeta^2} \qquad\qquad \eta_{e1} = \frac{n_{o1}}{n_{e1}}\sqrt{n_{e1}^2 - \zeta^2} \tag{A.2}$$

$$\eta_{o2} = \sqrt{n_{o2}^2 - \zeta^2} \qquad\qquad \eta_{e2} = \frac{n_{o2}}{n_{e2}}\sqrt{n_{e2}^2 - \zeta^2}$$

The Fresnel coefficients for each interface are given by the following equations for the p- and s- polarizations:

$$r_{\phi 1p} = \frac{-\left(\eta_{o1}^2\eta_\phi - \eta_\phi^2\eta_{e1}\right)}{\left(\eta_{o1}^2\eta_\phi + n_\phi^2\eta_{e1}\right)} \qquad\qquad r_{12p} = \frac{-\left(n_{o2}^2\eta_{e1} - n_{o1}^2\eta_{e2}\right)}{\left(n_{o2}^2\eta_{e1} + n_{o1}^2\eta_{e2}\right)} \tag{A.3}$$

$$r_{\phi 1s} = \frac{\left(\eta_\phi - \eta_{o1}\right)}{\left(\eta_\phi + \eta_{o1}\right)} \qquad\qquad r_{12s} = \frac{\left(\eta_{o1} - \eta_{o2}\right)}{\left(\eta_{o1} + \eta_{o2}\right)} \tag{A.4}$$

For a single anisotropic film on top of an anisotropic bulk phase, the phase thickness β for the p- and s- polarizations are given by

$$\beta_p = \frac{4\pi}{\lambda_0} d\eta_{e1} \tag{A.5}$$

$$\beta_s = \frac{4\pi}{\lambda_0} d\eta_{o1} \tag{A.6}$$

The final reflected amplitudes for the p- and s- polarizations are then given by substituting equations (A.3-A.6) into equation (A.1). Using equation (1) the amplitude and phase of the ellipsometric ratio can thus be calculated as

$$\Psi = \tan^{-1}\left(\left|\frac{R_p}{R_s}\right|\right) \tag{A.7}$$

$$\Delta = \arg\left(\frac{R_p}{R_s}\right) \tag{A.8}$$

For multiple layers, the calculation for reflection coefficients is more complicated than calculations for a single film given above. Most of the calculations for multilayers are performed using matrix methods where each layer is represented by two 2 x 2 matrices, one for the p- and one for s- polarizations. The Abelès formulation is a commonly used method of data analysis. The mth layer is represented by the two matrices and the characteristic matrix for a stack of layers is then determined by matrix multiplication. Consider figure 7. If the subscripts for medium air is "ϕ" and for bulk (substrate) is "s", from equations (A.2) the equation for the air interface is

$$n_{\phi}, \eta_0$$

1

2

$$i \qquad\qquad n_{oi}, n_{ei}$$

$$j \qquad\qquad n_{oj}, n_{ej}$$

$$\updownarrow d$$
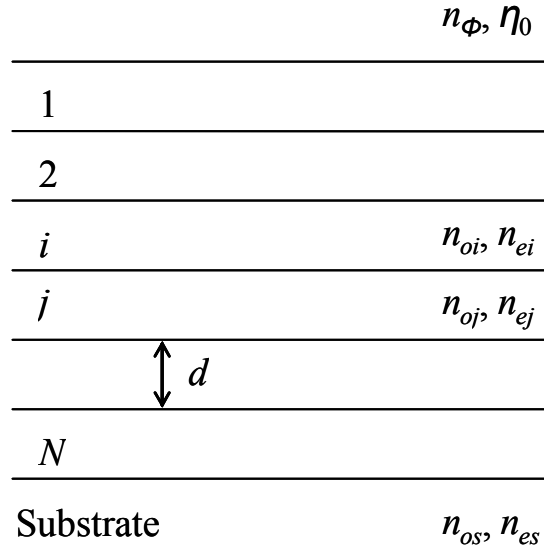
$$N$$

Substrate $\qquad\qquad n_{os}, n_{es}$

Figure 7 The model used in the Abelès matrix calculation of N strata where each stratum has thickness d.

$$\eta_{\phi} = \sqrt{n_0^2 - \zeta^2} \qquad\qquad\qquad (A.9)$$

For the anisotropic substrate, i.e. layer $(N+1)$

$$\eta_{os} = \sqrt{n_{os}^2 - \zeta^2} \qquad\qquad \eta_{es} = \frac{n_{os}}{n_{es}}\sqrt{n_{es}^2 - \zeta^2} \qquad\qquad (A.10)$$

and for the sub-layers, i.e. layer i,

$$\eta_{oi} = \sqrt{n_{oi}^2 - \zeta^2} \qquad\qquad \eta_{ei} = \frac{n_{oi}}{n_{ei}}\sqrt{n_{ei}^2 - \zeta^2} \qquad\qquad (A.11)$$

From equations (A.3) and (A.5), the Fresnel factors and phase angle for the *p*-polarization are

$$r_{\phi 1,p} = \frac{-\left(\eta_{o1}^2\eta_\phi - \eta_\phi^2\eta_{e1}\right)}{\left(\eta_{o1}^2\eta_\phi + n_\phi^2\eta_{e1}\right)} \qquad\qquad r_{ij,p} = \frac{-\left(n_{oj}^2\eta_{ei} - n_{oi}^2\eta_{ej}\right)}{\left(n_{oj}^2\eta_{ei} + n_{oi}^2\eta_{ej}\right)} \tag{A.12}$$

$$\beta_{i,p} = \frac{4\pi}{\lambda_0}d\eta_{ei} \tag{A.13}$$

From equations (A.6) and (A.8), the Fresnel factors and phase angle for the *s*-polarization are

$$r_{\phi 1,s} = \frac{\left(\eta_\phi - \eta_{o1}\right)}{\left(\eta_\phi + \eta_{o1}\right)} \qquad\qquad r_{ij,s} = \frac{\left(\eta_{oi} - \eta_{oj}\right)}{\left(\eta_{oi} + \eta_{oj}\right)} \tag{A.14}$$

$$\beta_{i,s} = \frac{4\pi}{\lambda_0}d\eta_{oi} \tag{A.15}$$

where $j = i+1$ and $i = 1..N$. Note that for $j = N+1$, $n_{oj} = n_{os}$, $n_{ej} = n_{es}$, $\eta_{oj} = \eta_{os}$, $\eta_{ej} = \eta_{es}$, i.e. regard $N+1$ as the substrate. For either *p*- or *s*-polarization, the calculation proceeds by doing the following matrices for $i > \phi$ and $i \leq N$,

$$M_\phi = \begin{bmatrix} 1 & r_{\phi 1} \\ r_{\phi 1} & 1 \end{bmatrix} \qquad\qquad M_i = \begin{bmatrix} \exp(i\beta) & r_{ij}\exp(i\beta) \\ r_{ij}\exp(-i\beta) & \exp(-i\beta) \end{bmatrix} \tag{A.16}$$

23

$$M = \begin{bmatrix} m_{11} & m_{12} \\ m_{21} & m_{22} \end{bmatrix} = M_0 M_1 M_2 ..... M_N = \prod_{i=0}^{N} M_i \tag{A.17}$$

and

$$R_p, R_s = \frac{m_{21}}{m_{11}} \tag{A.18}$$

to get the overall p- or s- Fresnel coefficient. The ellispometric parameters can be calculated from equations (A.7) and (A.8). (Note that this calculation method has been checked by showing it to be numerically equivalent to the 4 x 4 Berreman matrix calculation [24] extended by CN for a uniaxial film on top of a uniaxial substrate).

References

[1] Beaglehole D., Mol. Cryst. Liq. Cryst. **89** 319 (1982)

[2] Kocevar K., Musevic I., Phys. Rev. E **65** 021703 (2002)

[3] Pershan P. S., Braslau A., Weiss A. H., Als-Nielson J., Phys. Rev. A **35** (11) 4800 (1987)

[4] Lau Y. G. J, Richardon R. M., Cubitt R., J. Chem. Phys. **124** 234910 (2006)

[5] Azzam R. M. A., Bashara N. M., *Ellipsometry and Polarized Light*, North-Holland (1987)

[6] Kasten H., Strobl G., J. Chem. Phys. **103** (15) 6768 (1995)

[7] Lucht R., Bahr Ch., Heppke G., Phys. Rev. E **62** (2) 2324 (2002)

[8] Lucht R., Bahr Ch., Heppke G., J. Phys. Chem. **102** 6861 (1998)

[9] Lucht R., Bahr Ch., Phys. Rev. Lett. **78** (18) 3487 (1997)

[10] Lau Y. G. J., et al, Liquid Crystals submitted

[11] Haller I., Prog. Solid State Chem. **10** 103 (1975)

[12] Berreman D. W., J. Opt. Soc. Am. **62** (4) 502 (1972)

[13] Den Engelsen D., J. Opt. Soc. Am. **61** (11) 1460 (1971)

[14] Odarich V. A., Fizikia **5** 102 (1991)

[15] Odarich V. A., Fizikia **5** 97 (1991)

[16] Winterbottom A. B., Kgl. Norske Vid. selsk, skr., **1**, 149 (1955)

[17] Cauchy L., Bill. Des. Sc. Math. **14** 9 (1830)

[18] Abelès F., Ann. Physique **5** 596 (1950)

[19] Woolam J. A., Johs B., Herzinger C. M., Hilfiker J. N., Synowicki R., Bungay C., , SPIE Proceedings **CR72** 3 (1999)

[20] Johs B., Woolam J. A., Herzinger C. M., Hilfiker J. N., Synowicki R., Bungay C., SPIE Proceedings **CR72** 29 (1999)

[21] Powell M. J. D., AERE Report 7477, Harwell UK (1973)

[22] Guo W. and Fung B. M., J. Chem. Phys. **95,** 3917-3923 (1991)

[23] McMillan W L, Phys. Rev **A6**, 936-947 (1972)

[24] Berreman D. W., J. Opt. Soc. Am. **62** (4) 502 (1972)